Journal of Vibration Engineering & Technologies (2023) 11:1–18
https://doi.org/10.1007/s42417-022-00555-3

ORIGINAL PAPER

Natural Vibration of Axially Graded Multi-cracked Nanobeams in Thermal Environment Using Power Series

Mainul Hossain[1] · **Jaan Lellep**[1]

Received: 19 January 2022 / Revised: 30 March 2022 / Accepted: 15 April 2022 / Published online: 25 May 2022

Abstract

Purpose In this study, a numerical investigation of the dynamic behavior of axially graded multi cracked nanobeams in a thermal environment is demonstrated. The nanobeam is axially graded where the material properties are varying exponentially from one end to another end. The nanobeam is subjected to thermal load due to temperature variation. Multiple open and stable cracks are considered on the beam.

Method Euler-Bernoulli beam theory and nonlocal theory of elasticity are employed for the modeling of the nanobeam. Each crack is modeled as a rotational spring. The power series solution technique is applied effectively to solve this problem.

Results Mode shape diagrams are illustrated for single and multiple cracks to analyze the effects of nonhomogeneity and thermal load on the vibration of cracked nanobeams. The effects of crack severity, crack location, and nonlocal parameter on the vibration of nanobeams are presented.

Conclusion Mode shapes of the single and multi-cracked nanobeams are diverse for the different values of nonhomogeneity of the material. The outcomes of this analysis are verified with the outcomes of other researchers in the existing literature.

Keywords Axially graded beams · Nonlocal theory · Power series solution · Mode shape · Multiple cracks · Thermal effect

Introduction

Nanomaterials have emerged as a potential element in numerous researches of modern science and technology. Nanomaterials [1] can be distinguished from their bulk counterparts by their exceptional properties such as high strength and stiffness, high thermal conductivity, etc. Because of these properties, nanomaterials become a very attractive component in the application of nano-scale electromechanical systems. During this application, nanomaterials are subjected to various forces such as compression, tension, and vibration. To overcome the adverse effects of these forces, effective modeling is very essential. The classical linear theory of elasticity is not sufficient for the analysis of nanomaterials, because this theory cannot incorporate the small-scale effect [2]. Therefore, researchers extensively used two different types of gradient elasticity theories [3–8] such as strain gradient theory and stress gradient theory. In strain gradient theory, the material response at a point depends not only on the classical strain but also on the strain gradients of differential orders. On the other hand, in stress gradient theory, the material response depends on the stress as well as on the stress gradients up to some orders. Nonlocal elasticity theory is one of the forms of stress gradient theory. Generally, the nonlocal elasticity theory is an integro-differential equation whose solution is difficult. Eringen [9] proposed equivalent differential nonlocal elasticity which has been widely accepted to analyze the nanomaterials.

In this paper, an axially graded [10–13] beam is considered as a kind of nonhomogeneous beam where the material properties are varying along the x-axis exponentially. The axially graded beam [14–16] is a type of composite where the material properties are varying smoothly from one end to another end for eliminate the stress concentration at any specific cross-section. The demand for new advanced materials is increasing day by day. The axially functionally graded material is one of the exceptional innovations

Jaan Lellep contributed equally to this work.

✉ Mainul Hossain
mainul.hossain@ut.ee

Jaan Lellep
jaan.lellep@ut.ee

[1] Institute of Mathematics and Statistics, University of Tartu, Narva mnt 18, Tartu 51009, Estonia

of recent science and technology that satisfy the growing demand for advanced materials having essential properties for high-quality design. In addition, these materials are a special type of composite that can mitigate the disadvantage of conventional composites.

In most cases, the thermal effect [17–19] is ignored in the research. A small change in temperature can change the dynamic behavior of the beam which may cause the failure of the beam. When heat is applied to a body, it stores energy in its atom as kinetic energy that increases the vibration of the atom against the intermolecular forces. Due to this vibration, atoms move away from each other which increases the material size. Due to the rise in temperature, expansion occurs. On the other hand, contraction occurs because of loss of temperature. This expansion or contraction is proportional to the change in temperature. This proportionality can be expressed as linear thermal expansion of the material. According to the assumption of thermo-elasticity, thermal strain can be added with mechanical strain linearly. That is why, the equation of equilibrium is compatible with the thermal load.

A crack is a newly created surface that partially separates the body. Crack is not only a common defect but also very difficult to control [20]. Multiple cracks also can occur in nanomaterials. Formulation of multiple cracks problem is difficult and analysis is time-consuming. Cracks can decrease stiffness and reduce the natural frequency [21–26]. Therefore, cracks affect the dynamic behaviors of structures significantly. Cracks can be detected by modal parameters, such as natural frequencies, mode shapes, and damping factors [27]. The mode shape of the vibration of nanomaterials is significantly changed by the presence of cracks. Mode shape is one of the popular techniques to detect a crack [28, 29]. The mode shape diagram is very sensitive to cracks. The lower mode shape is less sensitive than the higher mode shape. Mode shape also explains the effects of crack severity very effectively.

The vibration of nanobeam has been analyzed using several techniques. Roostai and Haghpanahi [30] studied the vibration of nanobeam with multiple cracks. They applied a modified exact solution technique to analyze the multi-cracked nanobeam. Similarly, Loghmani and Yazdi [31] examined the vibration of multi-cracked and stepped nanobeams. They employed the wave approach to analyze their model. Aria et al. [32] investigated the thermal vibration of cracked nanobeams on an elastic matrix. They described the effectiveness of the finite-element method to analyze the model. Esen et al. [33] represented free vibration of cracked FG microbeam embedded in elastic matrix with magnetic and thermal effect. They scrutinized this problem using the analytical method. Their results showed that the magnetic field could be used to eliminate the negative effects of the temperature. Basically, the exact solution technique, perturbation method [34, 35], differential quadrature method [36, 37], and differential transform method [38-40] are very popular among researchers to investigate the dynamic behavior of beams. Similarly, the power series solution technique [41] has been used by a limited number of researchers for analyzing the dynamic problem of structures. However, this technique is rare to study the multi-cracked nanobeam.

In this paper, the power series solution technique is applied to investigate the effects of crack severity, crack location, nonhomogeneity, thermal effect, nonlocal parameter, and different boundary conditions on the vibration of axially graded multi-cracked nanobeams. The governing equation is derived by applying the Euler–Bernoulli beam theory and the theory of nonlocal elasticity. The beam is considered axially graded from one end to another end. Thermal load is also applied axially. Multiple stable and open cracks are considered on the beam where each crack is replaced by a rotational spring for modeling. Mode shape diagrams are also analyzed to describe the effect of nonhomogeneity and thermal load on the vibration of cracked nanobeams. In this paper, the effects of single and multiple cracks, location of cracks, nonhomogeneity, temperature, and nonlocal parameter on the vibration of nanobeams are studied. The outcomes of this analysis are examined with the outcomes of other researchers in the existing literature.

Mathematical Model

Description of the Problem

The geometry of an axially graded multi-cracked nanobeam is illustrated in Fig. 1. The left endpoint of the beam is located at the origin of the coordinate system. The neutral axis of the beam overlaps with the x-axis and the height of the beam is placed along the z-axis. L, b, and h describe the length, width, and height of the beam, respectively. Multiple open cracks are considered at the distance of a_i to a_n from the left endpoint. The material of the beam is axially graded along the x-axis. E and ρ are the elasticity and

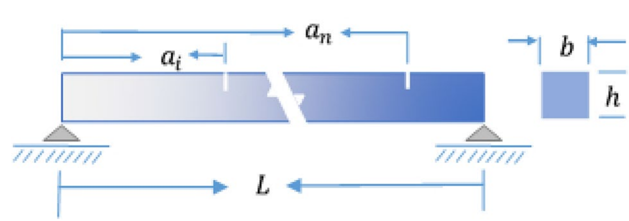

Fig. 1 An axially graded multi-cracked nanobeam

density varying exponentially from one end to another end. The objective of this analysis is to examine the natural vibration of axially graded multi-cracked nanobeams.

Beam Theory with Nonlocal Elasticity

Euler–Bernoulli beam theory is extensively acceptable to the researcher to analyze the structural elements. This theory is based on some assumptions [42–44] such as cross-sections of the beam are plane and perpendicular to the neutral axis during bending, transverse deformation is considered very small and shear deformation is neglected, and the beam is linearly elastic based on Hooke's law. According to the Euler–Bernoulli theory, the displacement fields [45] can be expressed as

$$V_1(x,z,t) = V(x,t) - z\frac{\partial W(x,t)}{\partial x} \tag{1}$$

$$V_2(x,z,t) = 0 \tag{2}$$

$$V_3(x,z,t) = W(x,t), \tag{3}$$

where V_1, V_2, and V_3 express the deflection in x, y, and z axis, respectively, and $W(x, t)$ and $V(x, t)$ define the transverse and axial deflection, respectively. One can write the axial strain as

$$\varepsilon_{xx} = \frac{\partial V}{\partial x} - z\frac{\partial^2 W}{\partial x^2}. \tag{4}$$

Considering axial load N and moment M, the Euler–Bernoulli equation for vibration can be presented as

$$\frac{\partial^2 M}{\partial x^2} + \frac{\partial}{\partial x}\left(N\frac{\partial W}{\partial x}\right) - m_0\frac{\partial^2 W}{\partial t^2} = 0, \tag{5}$$

where $m_0 = \rho A$ is the mass per unit length. However, this theory directly is not applicable to nanomaterials. The physical properties of nano-scale materials are different from macro-materials. To incorporate this scale effect, Eringen proposed the nonlocal theory of elasticity. According to his theory, the stress–strain relationship [46, 47] for a three-dimensional isotropic elastic solid can be expressed as

$$\sigma_{ij}(x) = \int_V \alpha(|\, x - x' \,|, \tau) t_{ij}(x') dV(x'), \tag{6}$$

where

$$t_{ij}(x') = \psi \varepsilon_{rr}(x')\delta_{ij} + 2\phi\varepsilon_{ij}(x'), \tag{7}$$

where ψ and ϕ represent Lame's constants. $t_{ij}(x')$ and $\varepsilon_{ij}(x')$ are the classical stress tensor and linear strain tensor at any point x' in the body, respectively. $\alpha(|\, x - x' \,|, \tau)$ represents the nonlocal modulus to indicate the nonlocal effects into the constitutive equation for the reference point x and source point x', respectively. In Eq. (6), $|\, x' - x \,|$ represents the Euclidean distance and τ can be presented as

$$\tau = \frac{e_0 a}{l}; \tag{8}$$

τ is a constant that indicates the ratio of internal and external characteristic length of the nanomaterial, where e_0 is the material constant. According to the theory of nonlocal elasticity, the integral constitutive relations can be transformed into the equivalent differential equation by substituting the kernel $\alpha(|\, x' - x \,|, \tau)$ as below

$$(1 - (e_0 a)^2 \Delta^2)\sigma_{kl} = t_{kl}, \tag{9}$$

where Δ^2 indicates the Laplacian operator. Nonlocal theory depends on internal characteristic length a. When a becomes zero, the nonlocal constitutive relations transform to the classical theory of elasticity. In the one-dimensional case, the nonlocal stress–strain relationship can be presented as

$$\sigma(x) - (e_0 a)^2 \frac{\partial^2 \sigma(x)}{\partial x^2} = E\varepsilon(x), \tag{10}$$

where $\sigma(x)$ and $\varepsilon(x)$ represent the stress and strain along the x-axis. Therefore, the nonlocal elasticity theory can be presented in terms of bending moment M, as follows:

$$M - (e_0 a)^2 \frac{\partial^2 M}{\partial x^2} = EI\left(-\frac{\partial^2 W}{\partial x^2}\right). \tag{11}$$

Combining the nonlocal theory (11) and Euler–Bernoulli theory (5) can be presented as

$$\begin{aligned}\frac{\partial^2}{\partial x^2}\left(EI\frac{\partial^2 W}{\partial x^2}\right) - (e_0 a)^2 \frac{\partial^2}{\partial x^2}\left[\rho A\frac{\partial^2 W}{\partial t^2} - \frac{\partial}{\partial x}\left(N\frac{\partial W}{\partial x}\right)\right] \\ - \frac{\partial}{\partial x}\left(N\frac{\partial W}{\partial x}\right) + \rho A\frac{\partial^2 W}{\partial t^2} = 0.\end{aligned} \tag{12}$$

Axially Graded Beam

An axially graded beam is a type of composite element that can avoid the point of stress concentration. It distributes stress gradually from one end to another end. Over the cross-section, the material properties are constant. Modulus of elasticity E and density ρ are varying along the length exponentially [48, 49]. These can be expressed as

$$E = E_0 e^{\lambda \frac{x}{L}}, \rho = \rho_0 e^{\lambda \frac{x}{L}}, \tag{13}$$

where E_0 and ρ_0 are the modulus of elasticity and density at the point $x = 0$, and λ is the coefficient of nonhomogeneity.

Thermal Load

Thermal load is created by the contraction and expansion of the material due to the temperature change. This load act as an axial load on the beam element. Thermal load [50] can be expressed as

$$N = -EA\alpha_t\theta. \tag{14}$$

Considering the varying modulus of elasticity, the thermal load can be presented as

$$N = -E_0 e^{\lambda \frac{x}{L}} A\alpha_t\theta, \tag{15}$$

where α_t is the coefficient of thermal expansion. According to the theory of Zarzycki 1982 and Kittel 1983 [51], the coefficient of thermal expansion can be presented as

$$\alpha_t = \frac{\gamma_G \rho c_V}{3E}, \tag{16}$$

where γ_G is the Grüneisen constant. Here, α_t depends on density and modulus of elasticity. Both of these parameters are varying equally along the x-axis. Therefore, α_t is constant over the length.

Modeling of Cracks

The mechanical properties of multiple open and stable cracks can be analyzed using the classical local stiffness model. According to this model, the beam is separated into two sub-beams for each crack at the crack position. Every crack in the beam is replaced by a mass-less rotational spring that connects the two neighboring segments together. In this model, the crack creates a discontinuity in the rotational angle at the location of the crack. Due to the presence of a crack, the beam achieves additional strain energy to the rotational spring. Strain energy is the result of bending moment and axial stress. The change of strain energy [32] can be presented as

$$\Delta s_c = \frac{1}{2}M\Delta\theta + \frac{1}{2}N\Delta u, \tag{17}$$

where M and N represent the bending moment and axial load respectively. $\Delta\theta$ indicates the rotational angle because of the spring and Δu represents the axial displacement at the location of the crack. Therefore, these can be expressed as

$$\Delta\theta = K_{MM}\frac{\partial^2 W}{\partial x^2} + K_{MN}\frac{\partial U}{\partial x} \tag{18}$$

$$\Delta u = K_{NN}\frac{\partial U}{\partial x} + K_{NM}\frac{\partial^2 W}{\partial x^2}, \tag{19}$$

where K_{MM}, K_{MN}, K_{NN}, and K_{NM} are the flexibility constants. When the beam is subjected to transverse vibration, longitudinal displacement Δu and the flexibility constants K_{MN}, K_{NN}, and K_{NM} are very small which can be neglected. Therefore, the discontinuity at the location of the crack can be expressed as

$$\Delta\theta = \frac{K_{MM}}{L}\frac{\partial^2 W(x)}{\partial x^2}\Big|_{x=a}, \tag{20}$$

where $\frac{K_{MM}}{L}$ can be replaced by K as

$$\Delta\theta = K\frac{\partial^2 W(x)}{\partial x^2}\Big|_{x=a}; \tag{21}$$

here, K is the crack severity. The crack severity depends on the crack depth and rotational spring stiffness. It can be expressed as follows [52]:

$$K = \frac{EI}{L}\frac{1}{\kappa_s}, \tag{22}$$

where κ_s is the spring stiffness. It can be written as

$$\kappa_s = \frac{EI}{h}\frac{1}{C(\gamma)}; \tag{23}$$

here, $\gamma = \frac{d_{cr}}{h}$ is the crack depth and beam height ratio. $C(\gamma)$ is the local compliance that can be computed from the strain energy density function as follows:

$$\begin{aligned} C(\gamma) = 5.346(&1.86\gamma^2 - 3.95\gamma^3 + 16.375\gamma^4 - 37.226\gamma^5 \\ &+ 76.81\gamma^6 \\ &- 126.9\gamma^7 + 172\gamma^8 - 143.97\gamma^9 + 66.56\gamma^{10}). \end{aligned} \tag{24}$$

Crack severity can be written from Eqs. (22) and (23) as

$$K = \frac{h}{L}C(\gamma). \tag{25}$$

Crack severity does not depend on the modulus of elasticity and density of the beam. Therefore, crack severity (K) is constant over the length of the axially graded beam.

Derivation of Governing Equation

In this paper, the beam is axially graded and also subjected to thermal load. Therefore, the material properties such as elasticity and density are varying along the x-axis. Similarly, the thermal load is also varying as an axial load. Considering these variations, Eq. (12) can be expressed as

$$\frac{\partial^2}{\partial x^2}\left(E(x)I\frac{\partial^2 W}{\partial x^2}\right)-(e_0a)^2\frac{\partial^2}{\partial x^2}\left[\rho(x)A\frac{\partial^2 W}{\partial t^2}-\frac{\partial}{\partial x}\left(N(x)\frac{\partial W}{\partial x}\right)\right]-\frac{\partial}{\partial x}\left(N(x)\frac{\partial W}{\partial x}\right)+\rho(x)A\frac{\partial^2 W}{\partial t^2}=0. \tag{26}$$

Applying the variable separation technique, deflection can be presented as

$$W(x,t)=\bar{W}(x)e^{i\omega_c t}. \tag{27}$$

Using the above function (27), the partial differential form (26) can be converted into the ordinary differential equation as

$$\frac{d^2}{dx^2}(E(x)I\frac{d^2\bar{W}}{dx^2})+(e_0a)^2\frac{d^2}{dx^2}(\rho(x)A{\omega_c}^2\bar{W})+(e_0a)^2\frac{d^3}{dx^3}\left(N(x)\frac{d\bar{W}}{dx}\right)-\frac{d}{dx}\left(N(x)\frac{d\bar{W}}{dx}\right)-\rho(x)A{\omega_c}^2\bar{W}=0. \tag{28}$$

Applying the conditions of nonhomogeneity and thermal effect from (13), (15), then Eq. (28) can be written as

$$E_0I\frac{d^2}{dx^2}\left(e^{\lambda\frac{x}{L}}\frac{d^2\bar{W}}{dx^2}\right)+(e_0a)^2\rho A{\omega_c}^2\frac{d^2}{dx^2}(e^{\lambda\frac{x}{L}}\bar{W})-(e_0a)^2E_0A\alpha_t\theta\frac{d^3}{dx^3}\left(e^{\lambda\frac{x}{L}}\frac{d\bar{W}}{dx}\right)+E_0A\alpha_t\theta\frac{d}{dx}\left(e^{\lambda\frac{x}{L}}\frac{d\bar{W}}{dx}\right)-\rho_0e^{\lambda\frac{x}{L}}A{\omega_c}^2\bar{W}=0. \tag{29}$$

After differentiating (29), it can be written as

$$E_0I\left(\frac{\lambda^2}{L^2}\frac{d^2\bar{W}}{dx^2}+2\frac{\lambda}{L}\frac{d^3\bar{W}}{dx^3}+\frac{d^4\bar{W}}{dx^4}\right)+(e_0a)^2\rho_0A{\omega_c}^2\left(\frac{\lambda^2}{L^2}\bar{W}+2\frac{\lambda}{L}\frac{d\bar{W}}{dx^2}\right)-(e_0a)^2E_0A\alpha_t\theta(\frac{\lambda^3}{L^3}\frac{d\bar{W}}{dx}+3\frac{\lambda^2}{L^2}\frac{d^2\bar{W}}{dx^2}+3\frac{\lambda}{L}\frac{d^3\bar{W}}{dx^3}+\frac{d^4\bar{W}}{dx^4})+E_0A\alpha_t\theta\left(\frac{\lambda}{L}\frac{d\bar{W}}{dx}+\frac{d^2\bar{W}}{dx^2}\right)-\rho_0A{\omega_c}^2\bar{W}=0 \tag{30}$$

The nondimensional parameters can be introduced as follows:

$$\xi=\frac{x}{L},w=\frac{\bar{W}}{L},\mu=\frac{e_0a}{L},n=\frac{E_0A\alpha_t\theta L^2}{E_0I},$$
$$\omega^2=(\bar{\omega})^4={\omega_c}^2L^4\frac{\rho_0A}{E_0I}.$$

Using the nondimensional parameters, Eq. (30) can be transformed as

$$\left(\lambda^2\frac{d^2w}{d\xi^2}+2\lambda\frac{d^3w}{d\xi^3}+\frac{d^4w}{d\xi^4}\right)+\mu^2\omega^2\left(\lambda^2w+2\lambda\frac{dw}{d\xi}+\frac{d^2w}{d\xi^2}\right)-\mu^2n(\lambda^3\frac{dw}{d\xi}+3\lambda^2\frac{d^2w}{d\xi^2}+3\lambda\frac{d^3w}{d\xi^3}+\frac{d^4w}{d\xi^4})+n\left(\frac{dw}{d\xi}+\frac{d^2w}{d\xi^2}\right)-\omega^2w=0 \tag{31}$$

Therefore, Eq. (31) can be presented in a simplified form as

$$\frac{d^4w}{d\xi^4}+\beta_1\frac{d^3w}{d\xi^3}+\beta_2\frac{d^2w}{d\xi^2}+\beta_3\frac{dw}{d\xi}+\beta_4w=0, \tag{32}$$

where

$$\beta_1=\frac{2\lambda-2\lambda\mu^2n}{1-\mu^2n},\beta_2=\frac{\lambda^2+\mu^2\omega^2-3\mu^2n\lambda^2+n}{1-\mu^2n},$$
$$\beta_3=\frac{2\mu^2\omega^2\lambda-\mu^2n\lambda^3+n}{1-\mu^2n},\beta_4=\frac{\mu^2\omega^2\lambda^2-\omega^2}{1-\mu^2n}.$$

In this nanobeam, multiple cracks are considered where n number of cracks separates the beam into $n+1$ segments. Finally, the governing equations for $n+1$ number of segments can be expressed as

$$\frac{d^4w_i}{d\xi^4}+\beta_1\frac{d^3w_i}{d\xi^3}+\beta_2\frac{d^2w_i}{d\xi^2}+\beta_3\frac{dw_i}{d\xi}+\beta_4w_i=0, \tag{33}$$

where $i=1,2,3,...,n+1$. Equation (33) represents the set of governing equations considering the $n+1$ segments that are separated at the location of cracks a_j. Where $j=1,2,...,n$. Boundary conditions for the beam can be presented as follows:

For the simply supported beam:

$$w_1(0)=0,\frac{d^2w_1(0)}{d\xi^2}=0,w_{n+1}(1)=0,\frac{d^2w_{n+1}(1)}{d\xi^2}=0.$$

For the fully clamped beam:

$$w_1(0)=0,\frac{dw_1(0)}{d\xi}=0,w_{n+1}(1)=0,\frac{dw_{n+1}(1)}{d\xi}=0.$$

For the clamped simply beam:

$$w_1(0) = 0, \frac{dw_1(0)}{d\xi} = 0, w_{n+1}(1) = 0, \frac{d^2 w_{n+1}(1)}{d\xi^2} = 0.$$

For the clamped free beam:

$$w_1(0) = 0, \frac{dw_1(0)}{d\xi} = 0, \frac{d^2 w_{n+1}(1)}{d^2\xi} = 0, \frac{d^3 w_{n+1}(1)}{d\xi^3} = 0.$$

In-between conditions at the location of cracks are as follows:

$$\begin{aligned}
&w_i(a_i) - w_{i+1}(a_i) = 0 \\
&\quad \frac{dw_i(a_i)}{d\xi} + K\frac{d^2 w_i(a_i)}{d\xi^2} - \frac{dw_{i+1}(a_i)}{d\xi} = 0 \\
&\quad \frac{d^2 w_i(a_i)}{d\xi^2} - \frac{d^2 w_{i+1}(a_i)}{d\xi^2} = 0 \\
&\frac{d^3 w_i(a_i)}{d\xi^3} + \mu^2\omega^2\frac{dw_i(a_i)}{d\xi} - \frac{d^3 w_{i+1}(a_i)}{d\xi^3} \\
&\quad - \mu^2\omega^2\frac{dw_{i+1}(a_i)}{d\xi} = 0.
\end{aligned}$$

One can solve these equations (33) by applying in-between conditions at the crack locations and any one set of end conditions for the boundary supports.

Power Series Solution

The power series solution [41] is a semi-analytical technique. In this technique, a power series is considered as a solution of the function. Therefore, the differential equation transforms into a set of algebraic equations. Linear, and nonlinear differential equations can be solved using the power series solution technique. Let us consider a series for the deflection of the beam as

$$w = \sum_{k=0}^{\infty} A_k \xi^k. \tag{34}$$

Similarly, derivatives of deflection can be written as

$$\frac{dw}{d\xi} = \sum_{k=1}^{\infty} kA_k \xi^{k-1} \tag{35}$$

$$\frac{d^2 w}{d\xi^2} = \sum_{k=2}^{\infty} k(k-1)A_k \xi^{k-2} \tag{36}$$

$$\frac{d^3 w}{d\xi^3} = \sum_{k=3}^{\infty} k(k-1)(k-2)A_k \xi^{k-3} \tag{37}$$

$$\frac{d^4 w}{d\xi^4} = \sum_{k=4}^{\infty} k(k-1)(k-2)(k-3)A_k \xi^{k-4}. \tag{38}$$

Substituting above derivatives into Eq. (33) as follows:

$$\begin{aligned}
&\sum_{k=4}^{\infty} k(k-1)(k-2)(k-3)A_k \xi^{k-4} \\
&\quad + \beta_1 \sum_{k=3}^{\infty} k(k-1)(k-2)A_k \xi^{k-3} \\
&\quad + \beta_2 \sum_{k=2}^{\infty} k(k-1)A_k \xi^{k-2} \\
&\quad + \beta_3 \sum_{k=1}^{\infty} kA_k \xi^{k-1} + \beta_4 \sum_{k=0}^{\infty} A_k \xi^k = 0.
\end{aligned} \tag{39}$$

Shifting the power of ξ, Eq. (39) can be written as

$$\begin{aligned}
&\sum_{k=0}^{\infty} (k+4)(k+3)(k+2)(k+1)A_{k+4}\xi^k \\
&\quad + \beta_1 \sum_{k=0}^{\infty} (k+3)(k+2)(k+1)A_{k+3}\xi^k \\
&\quad + \beta_2 \sum_{k=0}^{\infty} (k+2)(k+1)A_{k+2}\xi^k \\
&\quad + \beta_3 \sum_{k=0}^{\infty} (k+1)A_{k+1}\xi^k \\
&\quad + \beta_4 \sum_{k=0}^{\infty} A_k \xi^k = 0.
\end{aligned} \tag{40}$$

Equating the coefficients of ξ^k can be expressed as

$$\begin{aligned}
&(k+4)(k+3)(k+2)(k+1)A_{k+4} \\
&\quad + \beta_1(k+3)(k+2)(k+1)A_{k+3} \\
&\quad + \beta_2(k+2)(k+1)A_{k+2} + \beta_3(k+1)A_{k+1} \\
&\quad + \beta_4 A_k = 0.
\end{aligned} \tag{41}$$

Simplifying Eq. (41) can be written as

$$\begin{aligned}
A_{k+4} = &-\frac{\beta_1}{(k+4)}A_{k+3} \\
&- \frac{\beta_2}{(k+4)(k+3)}A_{k+2} \\
&- \frac{\beta_3}{(k+4)(k+3)(k+2)}A_{k+1} \\
&- \frac{\beta_4}{(k+4)(k+3)(k+2)(k+1)}A_k.
\end{aligned} \tag{42}$$

Using the above relation (42), one can calculate the series coefficients as follows:

$$A_4 = -\frac{1}{4}\beta_1 A_3 - \frac{1}{12}\beta_2 A_2 - \frac{1}{24}\beta_3 A_1 - \frac{1}{24}\beta_4 A_0 \tag{43}$$

$$A_5 = \frac{1}{20}(\beta_1^2 - \beta_2)A_3 + \frac{1}{60}(\beta_1\beta_2 - \beta_3)A_2 + \frac{1}{120}(\beta_1\beta_3 - \beta_4)A_1 + \frac{1}{120}\beta_1\beta_4 A_0 \tag{44}$$

$$\begin{aligned} A_6 = &-\frac{1}{120}(\beta_1^3 - 2\beta_1\beta_2 + \beta_3)A_3 \\ &- \frac{1}{360}(\beta_1^2\beta_2 - \beta_1\beta_3 - \beta_2^2 + \beta_4)A_2 \\ &- \frac{1}{720}(\beta_1^2\beta_3 - \beta_1\beta_4 - \beta_2\beta_3)A_1 - \frac{1}{720}(\beta_1^2\beta_4 - \beta_2\beta_4)A_0. \end{aligned} \tag{45}$$

Applying the series coefficients, the solution for the each segment of the beam can be written as

$$w_i = A_{i,0} + A_{i,1}\xi + A_{i,2}\xi^2 + A_{i,3}\xi^3 + \sum_{k=4}^{\infty} A_{i,k}\xi^k, \tag{46}$$

where $i = 1, ..., n+1$. Using the simply supported boundary conditions and intermediate conditions for cracks, one can eliminate constant coefficients ($A_{i,k}$) and solve these equations to form matrix as follows:

$$\begin{bmatrix} m_{1,1} & \cdots\ \cdots & m_{1,4(n+1)} \\ \cdots & \cdots\ \cdots & \cdots \\ \cdots & \cdots\ \cdots & \cdots \\ m_{4(n+1),1} & \cdots\ \cdots & m_{4(n+1),4(n+1)} \end{bmatrix} \begin{bmatrix} A_{1,0} \\ \cdots \\ \cdots \\ A_{(n+1),3} \end{bmatrix}. \tag{47}$$

The value of natural frequency for multi-cracked nanobeams can be determined by solving the above matrix. In this paper, single, double, and triple cracked nanobeams are analyzed.

Numerical Results and Discussion

In this section, parametric analysis is performed to scrutinize their impacts on the natural frequency of axially graded multi-cracked nanobeams in a thermal environment. First of all, the efficiency of the solution technique is measured by comparing the obtained results with the results of relevant papers in the existing literature. In addition, the influences of crack position on the various modes of natural frequency for several values of the gradient parameter are studied and presented graphically. Moreover, the effects of temperature and nonhomogeneity on the frequency ratio of intact and cracked nanobeams are illustrated. Furthermore, the effects of temperature, nonhomogeneity, and nonlocal parameter on the natural frequency are presented in tabular forms. Finally, the mode shapes are depicted to investigate the axially graded multi-cracked nanobeam with different support conditions, and to study the effects of nonhomogeneity, temperature, and a number of cracks on the transverse deflection.

Comparison of Results

In this section, the outcomes of the study are compared with the outcomes of some benchmark studies in the existing literature. This comparison is performed by investigating the effects of nonlocal parameter (μ), thermal load (n), and crack severity on different modes of natural frequency. In Table 1, the first mode of natural frequency (square root) for simply supported and fully clamped nanobeam is presented. The effect of crack is not considered as well as the beam is considered uniform and homogeneous in this section of calculation. Different values of nonlocal parameter (μ) and thermal load (n) are considered. It is understandable from these tabular data that natural frequency decreases for the increase of the nonlocal parameter. Therefore, the natural frequency increases for the decrease of temperature. Outcomes are verified with the results of Esen et al. [33] and Aria et al. [32] where they analyzed the cracked nanobeam on elastic matrix with temperature. During this comparison, specific results are selected from their paper where those data ignore the effects of crack and elastic matrix. Similarly, in Table 2, different modes of natural frequency (square root) for simply supported single cracked nanobeam are demonstrated. Nonhomogeneity of nanobeam is ignored in this section of calculation. Different values of crack positions (a), crack severity (K), and nonlocal parameter (μ) are also considered. It is comprehensible from these tabular data that the natural frequency decreases for the increase of crack severity. Frequency shows the lower value at the crack position of $a = 0.5$ than $a = 0.25$. This table data also matched with the results of Esen et al. [33] and Aria et al. [32]. However, specific tabular data are selected from their paper where these data ignore the effect of elastic matrix and temperature. These evaluations show a good understanding of these outcomes. In Table 3, different modes of natural frequency for a double-cracked beam with different values of the nonlocal parameter and crack severity are studied. Two cracks in the beam are located at $a_1 = 0.3$ and $a_2 = 0.7$, respectively. It is obvious from these tabular data that frequency decreases with the increases of the nonlocal parameter. The crack severity and boundary supports also influence the values of frequency. These table data also compare with the results of Roostai and Haghpanahi [30]. This comparison shows a close match among these results.

Effect of Crack Locations

The crack location is also crucial like crack severity for analyzing the cracked beam. In Figs. (2, 3, 4 and 5), different

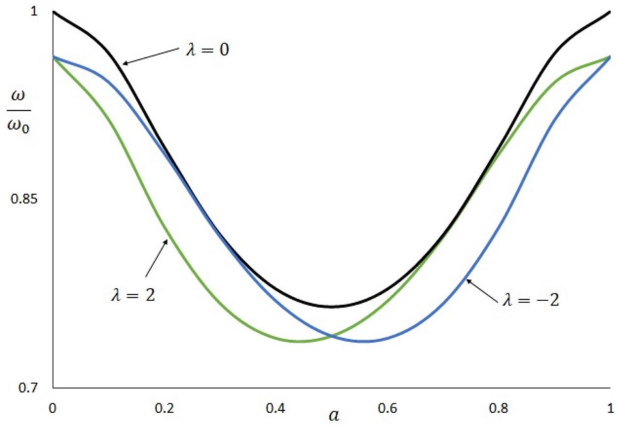

Fig. 2 Frequency ratio versus crack position (SS, 1st Mode)

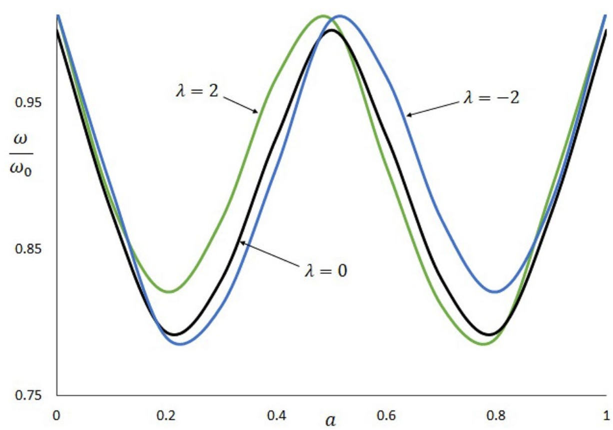

Fig. 3 Frequency ratio versus crack position (SS, 2nd Mode)

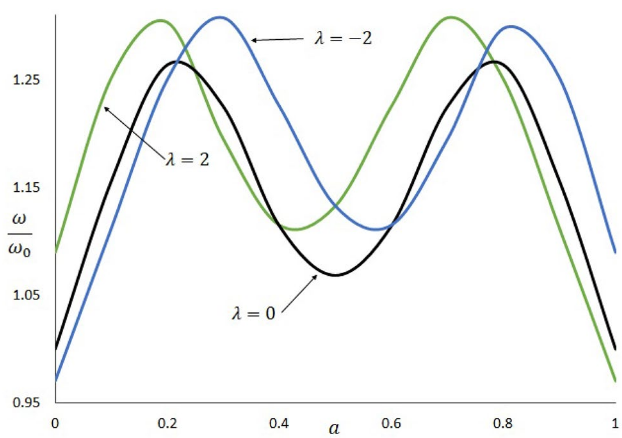

Fig. 4 Frequency ratio versus crack position (CC, 1st Mode)

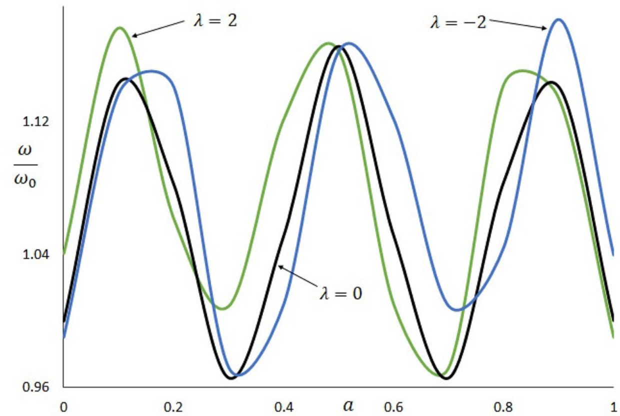

Fig. 5 Frequency ratio versus crack position (CC, 2nd Mode)

modes of frequency and two different support systems such as simply supported and fully clamped nanobeam are demonstrated. Thermal load is ignored in this section of the calculation. The frequency ratio is calculated by the frequency at any point with nonhomogeneity and the frequency at the initial point without considering nonhomogeneity. In this section, nonlocal parameter $\mu = 0.1$ and crack severity $K = 0.35$ are applied. It is evident from these figures that in the case of simply supported and the first mode of frequency, the frequency ratio slightly decreases for the presence of nonhomogeneity. However, in other cases, frequency increases with the presence of nonhomogeneity. It is very important in these curves that the frequency ratio is not affected by the positive or negative sign of nonhomogeneity. The effect of crack location is also influenced by the end support systems.

Frequency for Axially Graded Intact and Cracked Nanobeams Under Thermal Load

In Table 4, the natural frequency for a triple cracked beam with several values of the nonlocal parameter and crack severity is demonstrated. Three specific cracks are considered at the position of $a_1 = 0.3$, $a_2 = 0.5$, and $a_3 = 0.7$, respectively. The effects of nonhomogeneity and temperature are not considered. It is understandable in these tabular data that the frequency decreases for the increase of the value of the nonlocal parameter and crack severity. In this section, Table 5 and Table 6 represent the effect of temperature on natural frequency for axially graded intact or cracked nanobeam, respectively. The interactions between temperature, nonhomogeneity, nonlocal parameter, end supports, and different modes of frequency of intact and cracked nanobeam

Table 1 Natural frequency (square root) for varying nonlocal parameter, thermal load, and different end supports

SS	$\mu = 0$			$\mu = 0.1$			$\mu = 0.2$		
n	Present	[33]	[32]	Present	[33]	[32]	Present	[33]	[32]
3	2.8699	2.8696	2.8694	2.7725	2.7718	2.7714	2.5192	2.5182	2.5179
2	2.9688	2.9672	2.9680	2.8815	2.8810	2.8800	2.6606	2.6601	2.6599
1	3.0589	3.0575	3.0563	2.9793	2.9791	2.9787	2.7829	2.7825	2.7823
0	3.1416	3.1416	3.1415	3.0684	3.0683	3.0680	2.8908	2.8906	2.8903
− 1	3.2184	3.2173	3.2180	3.1505	3.1504	3.1501	2.9880	2.9880	2.9875
− 2	3.2901	3.2896	3.2894	3.2268	3.2266	3.2262	3.0765	3.0763	3.0759
− 3	3.3574	3.3570	3.3562	3.2978	3.2975	3.2973	3.1581	3.1575	3.1574
CC									
3	4.6404	4.6401	4.6397	4.4697	4.4698	4.4689	4.0511	4.0511	4.050
2	4.6706	4.6704	4.6696	4.5124	4.5126	4.5117	4.1303	4.1302	4.1296
1	4.7006	4.7003	4.6993	4.5541	4.5536	4.5532	4.2053	4.2051	4.2047
0	4.7300	4.7301	4.7292	4.5943	4.5941	4.5936	4.2767	4.2763	4.2759
− 1	4.7588	4.7575	4.7582	4.6336	4.6336	4.633	4.3444	4.344	4.3436
− 2	4.7871	4.7868	4.7861	4.6723	4.6718	4.6713	4.4091	4.4091	4.4084
− 3	4.8147	4.8145	4.814	4.7097	4.7091	4.7087	4.4710	4.4708	4.4703

Table 2 Natural frequency (square root) for simply supported cracked nanobeams in different modes with varying nonlocal parameter

a	K	mode	$\mu = 0.0$			$\mu = 0.2$		
			Present	[33]	[32]	Present	[33]	[32]
0.5	0	1	3.1416	3.1413	3.1409	2.8908	2.8907	2.8907
		2	6.2833	6.2830	6.2818	4.9582	4.9580	4.9578
		3	9.4236	9.4235	9.4228	6.4520	6.4520	6.4517
	0.065	1	3.0469	3.0467	3.0466	2.8032	2.8030	2.8030
		2	6.2833	6.2824	6.2818	4.9582	4.9580	4.9578
		3	9.1673	9.1657	9.1652	6.2603	6.2603	6.2601
	0.35	1	2.7496	2.7493	2.7489	2.5232	2.5232	2.5232
		2	6.2833	6.2825	6.2819	4.9582	4.9580	4.9578
		3	8.6129	8.6121	8.6114	5.7891	5.7890	5.7889
	2	1	2.0960	2.0959	2.0958	1.9099	1.9098	1.9098
		2	6.2833	6.2825	6.2818	4.9582	4.958	4.9578
		3	8.0732	8.0726	8.0715	5.3416	5.3415	5.3413
0.25	0	1	3.1416	3.1416	3.1409	2.8908	2.8908	2.8908
		2	6.2833	6.2825	6.2818	4.9582	4.9580	4.9580
		3	9.4244	9.4235	9.4228	6.4520	6.4520	6.4519
	0.065	1	3.0921	3.0921	3.0925	2.8447	2.8446	2.8446
		2	6.1028	6.1026	6.1019	4.8102	4.8100	4.8100
		3	9.3018	9.3019	9.3005	6.3636	6.3638	6.3637
	0.35	1	2.9072	2.9068	2.9064	2.6646	2.6645	2.6645
		2	5.6491	5.6486	5.6484	4.4168	4.4169	4.4168
		3	9.0765	9.0756	9.0752	6.1924	6.1923	6.1923
	2	1	2.3493	2.3487	2.3465	2.1134	2.1134	2.1134
		2	5.1046	5.1045	5.1042	3.9906	3.9906	3.9906
		3	8.9009	8.9005	8.8993	6.0691	6.0691	6.0691

Table 3 Natural frequency for double-cracked beams with different values of nonlocal parameter and crack severity

		SS				CC			
		K = 0.0325		K = 0.075		K = 0.0325		K = 0.075	
μ	Mode	[30]	Present	[30]	Present	[30]	Present	[30]	Present
0	1	9.474	9.475	9.023	9.023	22.173	22.174	21.952	21.951
	2	37.335	37.338	34.986	34.986	58.51	58.504	55.228	55.223
	3	88.313	86.383	87.741	85.883	118.63	108.242	116.184	103.508
0.5	1	5.087	5.086	4.84	4.839	10.914	10.915	10.822	10.821
	2	11.306	11.306	10.542	10.542	16.246	16.247	15.139	15.138
	3	18.324	18.323	18.172	18.171	23.413	23.401	22.325	22.326
1	1	2.873	2.873	2.732	2.732	6.018	6.018	5.97	5.97
	2	5.858	5.858	5.46	5.459	8.362	8.363	7.786	7.786
	3	9.313	9.313	9.236	9.236	11.948	11.923	11.356	11.354
1.5	1	1.966	1.966	1.87	1.869	4.094	4.094	4.062	4.062
	2	3.932	3.932	3.665	3.665	5.606	5.606	5.219	5.218
	3	6.228	6.228	6.176	6.1762	7.999	7.998	7.597	7.597

are very diverse. Table 5 represents the relationship between the nonlocal parameter, thermal load, and nonhomogeneity in absence of crack. In this section, three different values of the nonlocal parameter, thermal load from − 2 to 2, and nonhomogeneity − 2 to 2 are considered. The effect of crack is ignored in this part of the calculation. It is very clear that the frequency decreases for the increase of the nonlocal parameter. On the other hand, frequency increases for the decrease of temperature. The relationship between thermal load, nonhomogeneity, and natural frequency is very fluctuating for the mode of frequency and end supports. Table 6 represents the relationship between the nonlocal parameter, thermal load, and nonhomogeneity in the presence of a crack. In this section, different values of the nonlocal parameter, thermal load, and nonhomogeneity are considered as like in Table 4. In addition, a crack is considered at crack location $a = 0.25$ with the crack severity $K = 0.35$. The relationship between thermal load, nonhomogeneity, and natural frequency becomes more changeable in the presence of crack for various modes of frequency and various support systems.

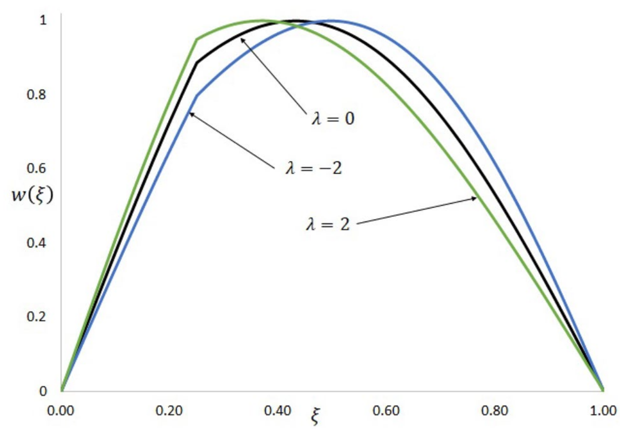

Fig. 6 Mode shape for different values of gradient parameter (1st mode, SS)

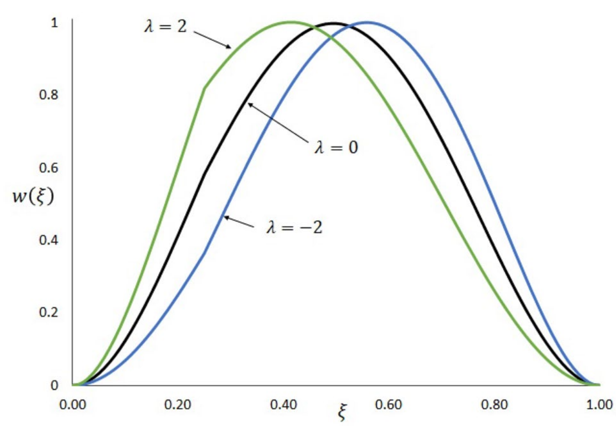

Fig. 7 Mode shape for different values of gradient parameter (1st mode, CC)

Mode Shape Illustration

Mode shape is one of the very important characteristics that explain the vibration of structural components. It describes the transverse displacement from the beam axis during vibration. It is a very significant measure that exhibits the pattern of vibration. In this section, the effects of nonhomogeneity, thermal load, and the number of cracks on the mode shape of cracked nanobeam are illustrated for different support systems. To understand the dynamic behavior of cracked nanobeam, mode shape analysis is necessary. In this section, three different sets of mode shape diagrams are presented for different values of nonhomogeneity and thermal

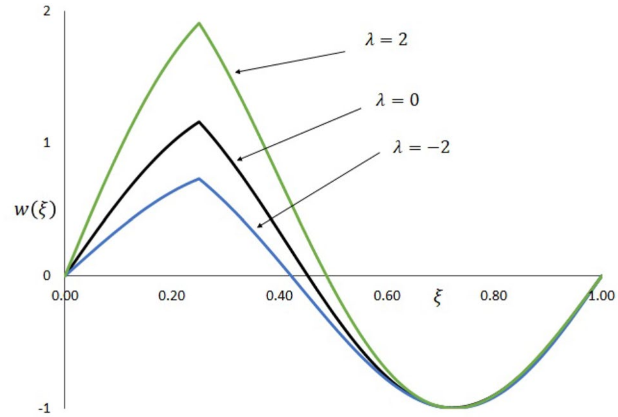

Fig. 8 Mode shape for different values of gradient parameter (2nd mode, SS)

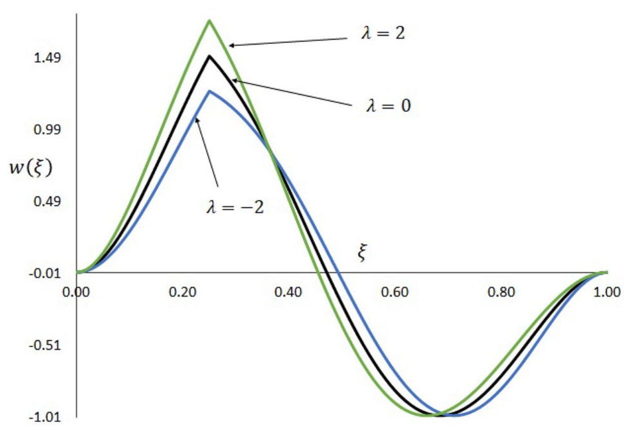

Fig. 9 Mode shape for different values of gradient parameter (2nd mode, CC)

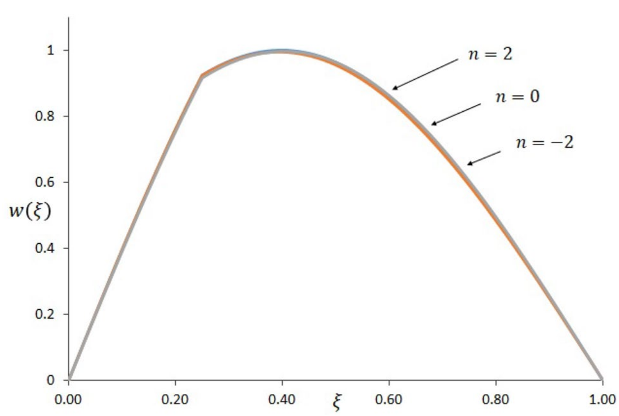

Fig. 10 Mode shape for different values of thermal load (1st mode, SS)

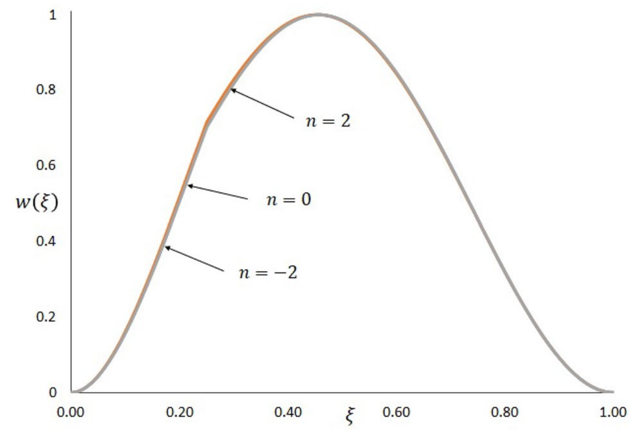

Fig. 11 Mode shape for different values of thermal load (1st mode, CC)

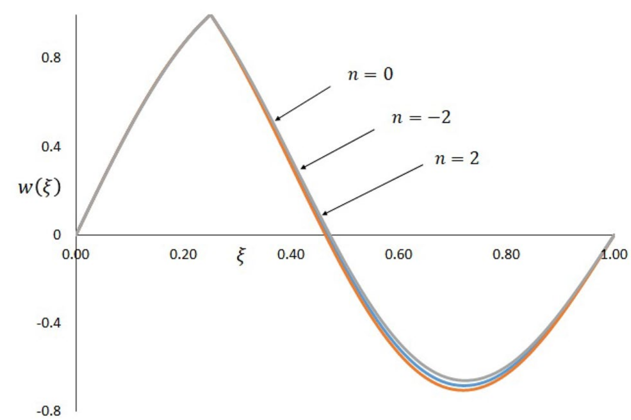

Fig. 12 Mode shape for different values of thermal load (2nd mode, SS)

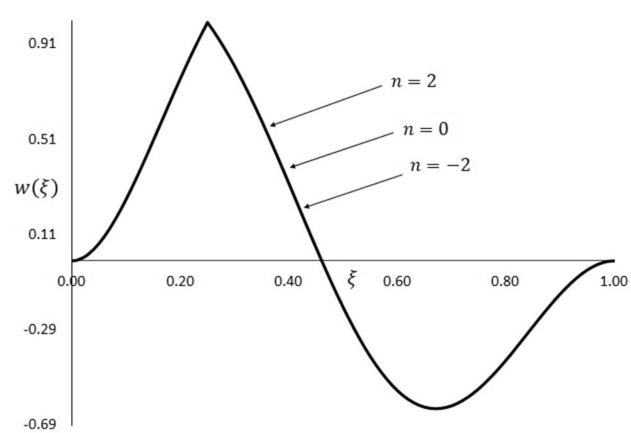

Fig. 13 Mode shape for different values of thermal load (2nd mode, CC)

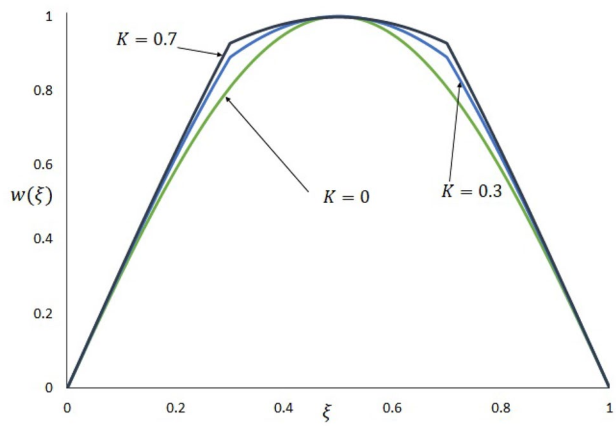

Fig. 14 Mode shape for double cracks and different values of crack severity (1st mode, SS)

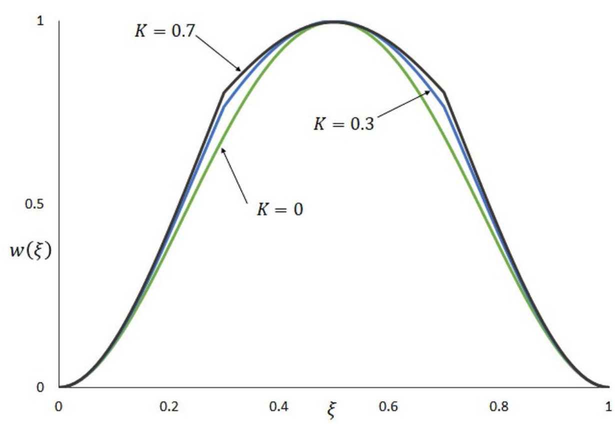

Fig. 15 Mode shape for double cracks and different values of crack severity (1st mode, CC)

load. In Figs. (6, 7, 8, 9, 10, 11, 12 and 13), different support conditions of the nanobeam are demonstrated where the location of crack $a = 0.25L$, value of the nonlocal parameter $\mu = 0.1$, and crack severity $K = 0.35$ are considered. Figures (6, 7, 8 and 9) represent mode shapes of axially graded cracked nanobeam for different values of nonhomogeneity. In this section of calculation, thermal load $n = 1$ is considered. Different values of nonhomogeneity $\lambda = 2$, $\lambda = 0$, and $\lambda = -2$ are applied. It is comprehensible from these figures that mode shapes of cracked nanobeam are considerably changed by the nonhomogeneity. Variation changes with the change of the value of nonhomogeneity. This variation also increases in the higher mode of frequency. Figures (9, 10, 11, 12 and 13) represent mode shapes of axially graded

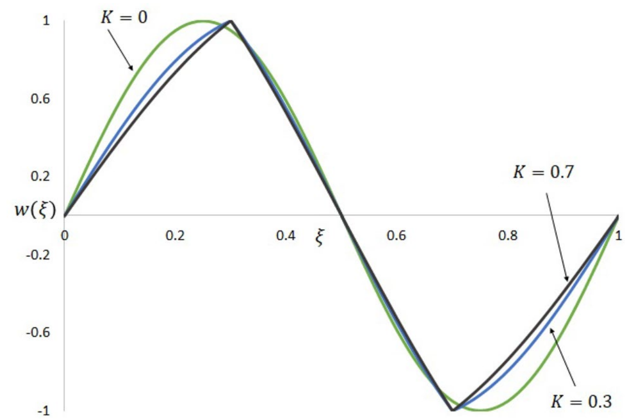

Fig. 16 Mode shape for double cracks and different values of crack severity (2nd mode, SS)

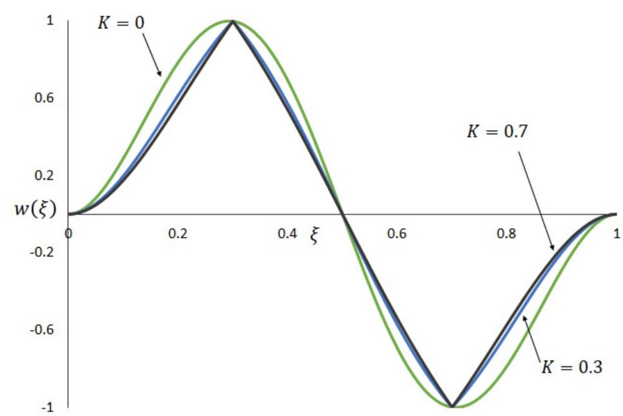

Fig. 17 Mode shape for double cracks and different values of crack severity (2nd mode, CC)

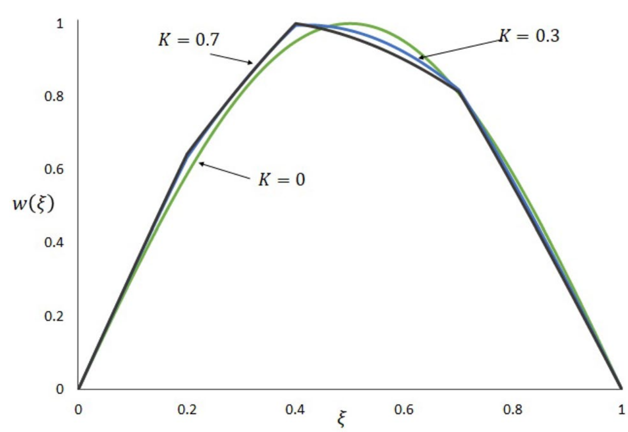

Fig. 18 Mode shape for triple cracks and different values of crack severity (1st mode, SS)

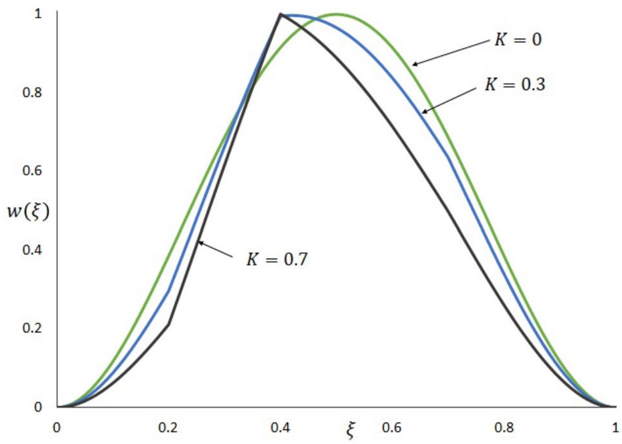

Fig. 19 Mode shape for triple cracks and different values of crack severity (1st mode, CC)

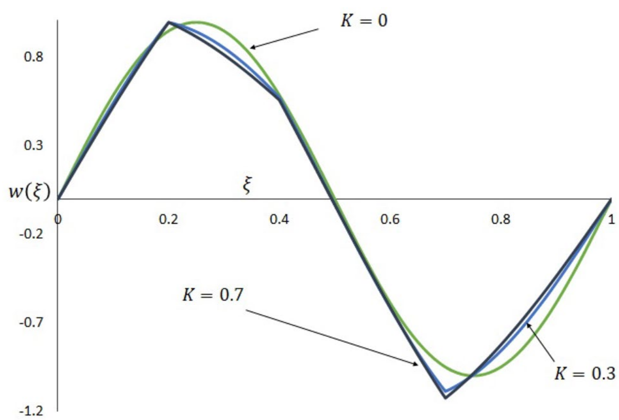

Fig. 20 Mode shape for triple cracks and different values of crack severity (2nd mode, SS)

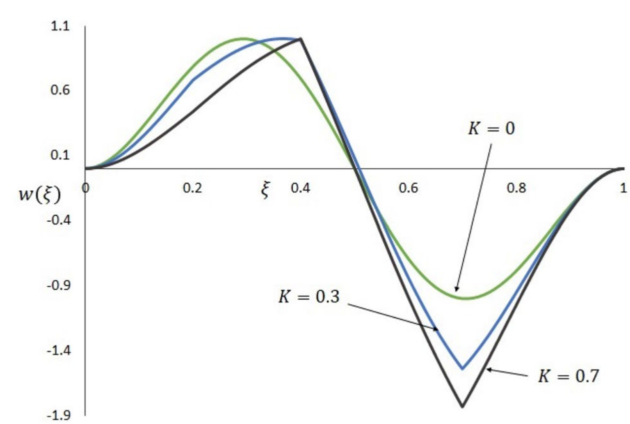

Fig. 21 Mode shape for triple cracks and different values of crack severity (2nd mode, CC)

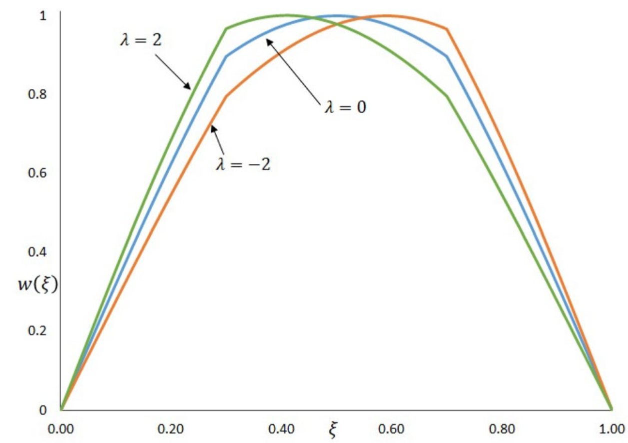

Fig. 22 Mode shape for double cracks and different values of nonhomogeneity (1st mode, SS)

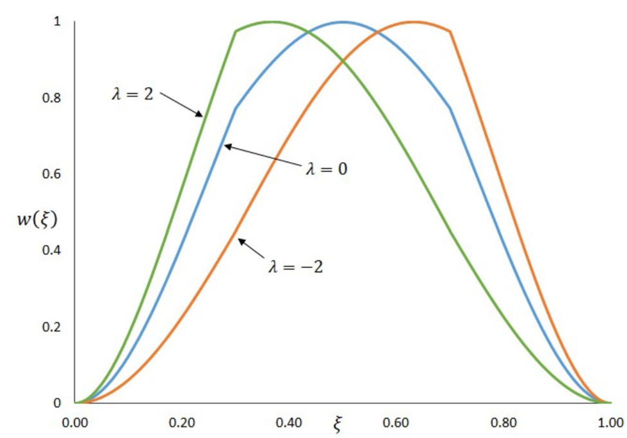

Fig. 23 Mode shape for double cracks and different values of nonhomogeneity (1st mode, CC)

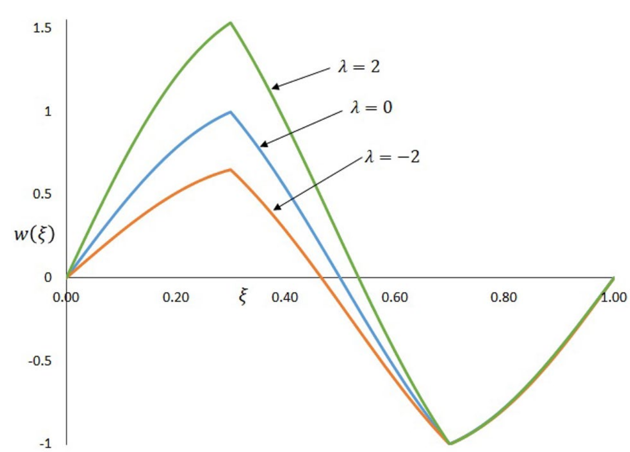

Fig. 24 Mode shape for double cracks and different values of nonhomogeneity (2nd mode, SS)

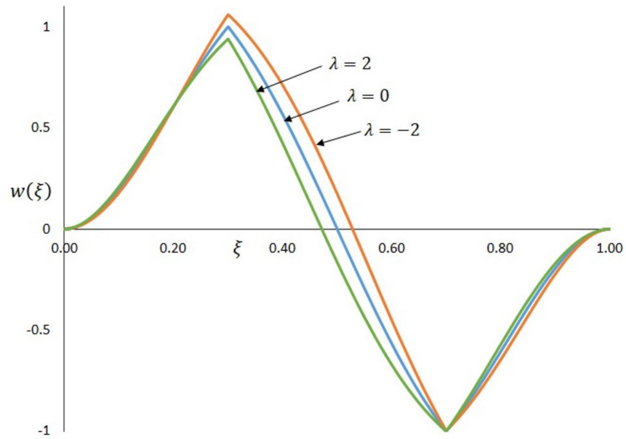

Fig. 25 Mode shape for double cracks and different values of nonhomogeneity (2nd mode, CC)

cracked nanobeam for various values of thermal load. In this section of calculation, nonhomogeneity $\lambda = 1$ is considered. Three different values of thermal load $n = 2, n = 0$, and $n = -2$ are applied. It is very clear from these figures that mode shapes are slightly influenced by the thermal load. It can be concluded that the nonhomogeneity is more effective on mode shape than the thermal load. Figures (14, 15, 16, 17, 18, 19, 20 and 21) represent the mode shapes of double and triple cracked nanobeam with fully clamped and simply supported boundary conditions. The nonhomogeneity and thermal effect are not considered. Three specific values of crack severity $K = 0$, $K = 0.3$, $K = 0.7$ are used. Figures (14, 15, 16 and 17) describe the mode shape for double-cracked nanobeam. Two similar cracks at $a = 0.3$ and $a = 0.7$ are considered. Similarly, Figs. (18, 19, 20 and 21) reveal the mode shape for triple cracked nanobeam. Three similar cracks at $a = 0.2$, $a = 0.4$, and $a = 0.7$ are considered, respectively. From these figures, it is seen that the number of cracks significantly changes the mode shape diagram. Figures (22, 23, 24 and 25) reveal the mode shapes of double-cracked nanobeam with various nonhomogeneity. In these figures, crack severity $K = 0.35$, crack locations $a = 0.3, b = 0.7$, nonlocal parameter $\mu = 0.1$, and thermal load $n = 0$ are considered. Three different values of nonhomogeneity are used in this analysis. It is evident that the mode shape is significantly affected by the nonhomogeneity of the beam.

Conclusion

In this study, the dynamic behavior of axially graded cracked nanobeams with thermal load is analyzed using the power series solution technique. Mode shapes have been illustrated to analyze the effects of nonhomogeneity and thermal load on the vibration of cracked nanobeams. The power series solution technique is employed to study the problem and to illustrate the mode shapes that analyze the natural vibration of multi-cracked nanobeams. Frequency is affected by the crack position as well as the nonhomogeneity. It is shown that the effects of nonhomogeneity and thermal load together on intact and cracked nanobeams are very diverse in different modes of frequency and different end supports. It is evident from these mode shape studies that mode shapes of the single- and multi-cracked nanobeams are very fluctuating for the nonhomogeneity of the material. The thermal load is less effective on the mode shape of cracked nanobeams than the

Table 4 Natural frequency for triple cracked nanobeams with several values of nonlocal parameter and crack severity

SS	K = 0.0325			K = 0.075			K = 0.15		
μ	1	2	3	1	2	3	1	2	3
0	9.203	37.338	83.977	8.506	34.986	80.523	7.585	31.717	75.231
0.5	4.941	11.306	17.692	4.563	10.542	16.655	4.063	9.452	14.897
1	2.79	5.858	8.992	2.576	5.459	8.459	2.293	4.891	7.555
1.5	1.909	3.932	6.013	1.763	3.665	5.656	1.569	3.282	5.050
CC									
0	21.708	58.508	107.492	21.037	55.223	102.602	20.182	50.941	94.695
0.5	10.622	16.247	22.545	10.229	15.138	20.393	9.699	13.683	17.589
1	5.846	8.363	11.522	5.622	7.786	10.405	5.310	7.029	8.977
1.5	3.975	5.606	7.704	3.821	5.218	6.966	3.606	4.709	6.011

Table 5 Frequency for several values of nonlocal parameter, thermal load, and nonhomogeneity without crack

SS	$K = 0$						
		$\mu = 0$			$\mu = 0.2$		
n	λ	1	2	3	1	2	3
− 2	− 2	10.3271	40.7773	90.3672	8.9497	26.4121	43.9336
	0	10.8252	40.4648	89.8203	9.4653	26.1387	43.7070
	2	10.5127	40.8320	90.3984	9.1021	26.4551	43.9570
0	− 2	9.48682	39.8555	89.3984	8.1079	24.9785	41.9179
	0	9.87012	39.4805	88.8203	8.3569	24.5839	41.6289
	2	9.48682	39.8555	89.3984	8.1079	24.9785	41.9179
2	− 2	8.58057	38.9004	88.4297	7.1704	23.4550	39.8008
	0	8.81396	38.4668	87.8203	7.0796	22.9199	39.4336
	2	8.33545	38.8496	88.3984	6.9741	23.4082	39.7773
CC							
− 2	− 2	23.3847	63.1211	122.5078	20.1465	38.6425	57.3867
	0	22.9160	62.4179	121.7109	19.4404	38.2832	57.0117
	2	23.4667	63.1523	122.5234	20.2012	38.6816	57.4023
0	− 2	22.9394	62.4258	121.7265	19.0732	36.8497	54.9414
	0	22.3730	61.6757	120.9141	18.2900	36.4238	54.5195
	2	22.9394	62.4258	121.7265	19.0732	36.8496	54.9570
2	− 2	22.4863	61.7148	120.9296	17.9365	34.9668	52.3789
	0	21.8144	60.9179	120.0859	17.0596	34.4629	51.9258
	2	22.3965	61.6836	120.9141	17.8779	34.9238	52.3711
CS							
− 2	− 2	18.2393	53.3008	107.8047	15.9443	33.5566	51.3945
	0	16.1475	50.8164	105.1484	13.8330	32.0215	50.1602
	2	14.2178	49.4023	103.8516	12.0615	31.2363	49.4883
0	− 2	17.7197	52.5273	106.9453	14.9365	31.8886	49.1133
	0	15.4189	49.9648	104.2422	12.7451	30.3379	47.8945
	2	13.3447	48.5273	102.9453	11.1084	29.6777	47.3164
2	− 2	17.1924	51.7383	106.0859	13.8545	30.1269	46.7148
	0	14.6514	49.0977	103.3359	11.5557	28.5527	45.5117
	2	12.4053	47.6367	102.0234	10.0654	28.0332	45.0352
CF							
− 2	− 2	5.51123	26.9238	67.0039	5.4624	21.0410	39.4961
	0	2.63501	22.5332	62.4023	2.8523	18.7393	38.6426
	2	–	18.7998	59.1367	1.2200	16.3994	40.4648
0	− 2	6.26221	26.5839	66.3712	5.8511	19.9512	37.6543
	0	3.51587	22.0332	61.6992	3.5793	17.5752	36.8144
	2	1.8405	18.1729	58.3867	2.4651	15.2314	38.7910
2	− 2	7.0054	26.2285	65.7383	6.2554	18.7822	35.7207
	0	4.2922	21.5097	60.9805	4.2810	16.2998	34.8926
	2	2.7434	17.5068	57.6367	3.4187	13.9228	37.0644

Table 6 Frequency for several values of nonlocal parameter, thermal load, and nonhomogeneity with crack

SS	$K = 0.35, a = 0.25$						
		$\mu = 0$			$\mu = 0.2$		
n	λ	1	2	3	1	2	3
− 2	− 2	9.1362	32.1699	82.4297	7.7495	20.2324	40.2070
	0	9.2583	32.7246	83.3203	7.9887	20.5723	40.1445
	2	8.6909	33.9824	85.3359	7.4907	21.3496	40.6367
0	− 2	8.4341	31.4004	81.5078	7.0942	19.2588	38.4238
	0	8.4517	31.9121	82.3828	7.1001	19.5088	38.3457
	2	7.8081	33.1894	84.3984	6.6812	20.3730	38.9394
2	− 2	7.6694	30.6113	80.5859	6.3442	18.2119	36.5410
	0	7.5503	31.0762	81.4297	6.0474	18.3486	36.4394
	2	6.7993	32.3809	83.4765	5.7388	19.3057	37.1426
CC							
− 2	− 2	23.2675	56.0664	107.3516	19.9434	32.5371	48.3789
	0	22.7676	54.0429	109.0234	19.3349	31.1934	49.1836
	2	22.4668	54.4414	112.4453	19.2568	31.5059	50.6836
0	− 2	22.7637	55.6289	106.6484	18.8388	31.6035	46.6523
	0	22.2715	53.5429	108.3047	18.2373	30.2949	47.3320
	2	22.0566	53.9258	111.7109	18.3467	30.5449	48.7930
2	− 2	22.2441	55.1836	105.9453	17.6709	30.5488	44.8633
	0	21.7598	53.0429	107.5703	17.0518	29.2871	45.4023
	2	21.6348	53.4102	110.9766	17.3545	29.4980	46.8398
CS							
− 2	− 2	17.8154	49.1445	92.8828	15.3779	30.5801	42.0586
	0	16.1475	45.3242	91.9922	13.8193	27.9941	41.6680
	2	14.0088	43.1211	92.6797	11.9385	26.6113	41.8867
0	− 2	17.1826	48.6211	92.1641	14.3291	29.5059	40.6055
	0	15.4014	44.7383	91.2109	12.7061	27.0293	40.1523
	2	13.1943	42.5039	91.8828	11.0303	25.7519	40.4102
2	− 2	16.5244	48.0898	91.4297	13.2002	28.2910	39.0820
	0	14.6084	44.1367	90.4141	11.4775	25.9316	38.5762
	2	12.3135	41.8711	91.0703	10.0303	24.7949	38.8730
CF							
− 2	− 2	4.0891	26.9238	59.1133	3.9822	21.0293	33.4121
	0	1.7064	22.3066	54.1367	1.8927	18.4951	31.8887
	2	–	18.0791	50.9101	–	15.3662	33.0097
0	− 2	4.8713	26.5839	58.7383	4.5183	19.9395	32.4980
	0	2.7737	21.8535	53.6836	2.8093	17.4111	31.0215
	2	1.4867	17.5381	50.4102	1.9977	14.3916	32.2480
2	− 2	5.6060	26.2246	58.3555	5.0298	18.7822	31.4629
	0	3.5969	21.3730	53.2148	3.5745	16.2217	30.0527
	2	2.4836	16.9619	49.8945	3.0383	13.2842	31.4394

nonhomogeneity. This analysis can be used to design nanoscale electromechanical systems.

Acknowledgements This research has been financed by the University of Tartu ASTRA Project PER ASPERA (European Regional Development Fund).

References

1. Behdad S, Fakher M, Hosseini-Hashemi S (2021) Dynamic stability and vibration of two-phase local/nonlocal VFGP nanobeams incorporating surface effects and different boundary conditions. Mech Mater 153:103633
2. Ahmadi I (2021) Vibration analysis of 2D-functionally graded nanobeams using the nonlocal theory and meshless method. Eng Anal Bound Elem 124:142–154
3. Faghidian SA (2018) Integro-differential nonlocal theory of elasticity. Int J Eng Sci 129:96–110
4. Faghidian SA (2020) Higher-order nonlocal gradient elasticity: a consistent variational theory. Int J Eng Sci 154:103337
5. Mikhasev G, Nobili A (2020) On the solution of the purely nonlocal theory of beam elasticity as a limiting case of the two-phase theory. Int J Solids Struct 190:47–57
6. Fuschi P, Pisano AA, Polizzotto C (2019) Size effects of small-scale beams in bending addressed with a strain-difference based nonlocal elasticity theory. Int J Mech Sci 151:661–671
7. Fazlali M, Moghtaderi SH, Faghidian SA (2021) Nonlinear flexure mechanics of beams: stress gradient and nonlocal integral theory. Mater Res Express 8:035011
8. Huang K, Cai X, Wang M (2020) Bernoulli-Euler beam theory of single-walled carbon nanotubes based on nonlinear stress-strain relationship. Mater Res Express 7:125003
9. Eringen AC (2002) Nonlocal continuum field theories. Springer-Verlag, New York Inc, New York
10. Datta P (2021) Active vibration control of axially functionally graded cantilever beams by finite element method. Mater Today Proceed 44:2543–2550
11. Zhang X, Ye Z, Zhou Y (2019) A Jacobi polynomial based approximation for free vibration analysis of axially functionally graded material beams. Compos Struct 225:111070
12. Li Z, Song Z, Yuan W, He X (2021) Axially functionally graded design methods for beams and their superior characteristics in passive thermal buckling suppressions. Compos Struct 257:113390
13. Šalinić S, Obradović A, Tomović A (2018) Free vibration analysis of axially functionally graded tapered, stepped, and continuously segmented rods and beams. Compos Part B 150:135–143
14. Changjian J, Linquan Y, Cheng L (2020) Transverse vibration and wave propagation of functionally graded nanobeams with axial motion. J Vib Eng Technol 8:257–266
15. Haonan L, Cheng S-P, Yao L (2021) Vibration analysis of rotating functionally graded piezoelectric nanobeams based on the nonlocal elasticity theory. J Vib Eng Technol 9:1155–1173
16. Tang Y, Ding Q (2019) Nonlinear vibration analysis of a bi-directional functionally graded beam under hygro-thermal loads. Compos Struct 225:111076
17. Jin Q, Ren Y, Peng F, Jiang H (2020) Imperfection sensitivity of free vibration of symmetrically/antisymmetrically laminated FRC beams in thermally pre-and post-buckling equilibrium states. Acta Astronautica 173:240–251
18. Xu J, Yang Z, Yang J, Li Y (2021) Free vibration analysis of rotating FG-CNT reinforced composite beams in thermal environments with general boundary conditions. Aerosp Sci Technol 118:107030
19. Beg MS, Yasin MY (2021) Bending, free and forced vibration of functionally graded deep curved beams in thermal environment using an efficient layer wise theory. Mech Mater 159:103919
20. Chen B, Lin B, Zhao X, Zhu W, Yang Y, Li Y (2021) Closed-form solutions for forced vibrations of a cracked double-beam system interconnected by a viscoelastic layer resting on Winkler-Pasternak elastic foundation. Thin-Walled Struct 163:107688
21. CholUk R, Qiang Z, ZhunHyok Z, ChungHyok C, YongIl S, KwangIl R (2021) Nonlinear dynamics simulation analysis of rotor-disc-bearing system with transverse crack. J Vib Eng Technol 9:1433–1445
22. Soni S, Jain NK, Joshi PV, Gupta A (2020) Effect of fluid-structure interaction on vibration and deflection analysis of generally orthotropic submerged micro-plate with crack under thermal environment: an analytical approach. J Vib Eng Technol 8:643–672
23. Agrawal AK, Chakraborty G (2021) Dynamics of a cracked Cantilever beam subjected to a moving point force using discrete element method. J Vib Eng Technol 9:803–815
24. Ahmadvand M, Asadi P (2021) Free vibration analysis of flexible rectangular fluid tanks with a horizontal crack. Appl Math Model 91:93–110
25. Shaat M, Khorshidi MA, Abdelkefi A, Shariati M (2016) Modeling and vibration characteristics of cracked nano-beams made of nanocrystalline materials. Int J Mech Sci 115–116:574–585
26. Chinka SSB, Putti SR, Adavi BK (2021) Modal testing and evaluation of cracks on cantilever beam using mode shape curvatures and natural frequencies. Structures 32:1386–1397
27. Kumar R, Singh SK (2021) Crack detection near the ends of a beam using wavelet transform and high resolution beam deflection measurement. Eur J Mech / A Solids 88:104259
28. Song M, Gong Y, Yang J, Zhu W, Kitipornchai S (2020) Nonlinear free vibration of cracked functionally graded graphene platelet-reinforced nanocomposite beams in thermal environments. J Sound Vib 468:115115
29. Wu Q, Guo S, Li X, Gao G (2020) Crack diagnosis method for a cantilevered beam structure based on modal parameters. Meas Sci Technol 31:035001
30. Roostai H, Haghpanahi M (2014) Vibration of nanobeams of different boundary conditions with multiple cracks based on nonlocal elasticity theory. Appl Math Modell 38:1159–1169
31. Loghmani M, Yazdi MRH (2018) An analytical method for free vibration of multi cracked and stepped nonlocal nanobeams based on wave approach. Results Phys 11:166–181
32. Aria AI, Friswell MI, Rabczuk T (2019) Thermal vibration analysis of cracked nanobeams embedded in an elastic matrix using finite element analysis. Compos Struct 212:118–128
33. Esen I, Özarpa C, Eltaher MA (2021) Free vibration of a cracked FG microbeam embedded in an elastic matrix and exposed to magnetic field in a thermal environment. Compos Struct 261:113552
34. Hossain M, Lellep J (2020) The effect of rotatory inertia on natural frequency of cracked and stepped nanobeam. Eng Res Express 2:035009
35. Hossain M, Lellep J (2021) Transverse vibration of tapered nanobeam with elastic supports. Eng Res Express 3:015019
36. Al-Furjan MSH, Hatami A, Habibi M, Shan L, Tounsi A (2021) On the vibrations of the imperfect sandwich higher-order disk with a lactic core using generalize differential quadrature method. Compos Struct 257:113150
37. Yan Y, Liu B, Xing Y, Carrera E, Pagani A (2021) Free vibration analysis of variable stiffness composite laminated beams and plates by novel hierarchical differential quadrature finite elements. Compos Struct 274:114364

38. Hossain MM, Lellep J (2021) Mode shape analysis of dynamic behaviour of cracked nanobeam on elastic foundation. Eng Res Express 3:045003
39. Lin Y, Chang KH, Chen CK (2020) Hybrid differential transform method/smoothed particle hydrodynamics and DT/finite difference method for transient heat conduction problems. Int Commun Heat Mass Transfer 113:104495
40. Areiza-Hurtado M, Aristizabal-Ochoa JD (2020) Large-deflection analysis of prismatic and tapered beam-columns using the Differential Transform Method. Structures 28:923–932
41. Soltani M, Asgarian B, Mohri F (2014) Elastic instability and free vibration analyses of tapered thin-walled beams by the power series method. J Construct Steel Res 96:106–126
42. Martin B, Salehian A (2020) Techniques for approximating a spatially varying Euler-Bernoulli model with a constant coefficient model. Appl Math Modell 79:260–283
43. Cardoso RPR (2020) A new beam element which blends the Euler-Bernoulli beam theory with idealised transverse shear flows for aircraft structural analysis. Thin-Walled Struct 157:107118
44. Malik S, Singh DK, Bansal G, Paliwal V, Manral AR (2021) Finite element analysis of Euler's Bernoulli cantilever composite beam under uniformly distributed load at elevated temperature. Mater Today Proceed 46:10725–10731
45. Yin S, Xiao Z, Deng Y, Zhang G, Liu J, Gu S (2021) Isogeometric analysis of size-dependent Bernoulli-Euler beam based on a reformulated strain gradient elasticity theory. Comput Struct 253:106577
46. Atanasov MS, Stojanovic V (2020) Nonlocal forced vibrations of rotating cantilever nano-beams. Eur J Mech / A Solids 79:103850
47. Adhikari S, Karlicic D, Liu X (2021) Dynamic stiffness of nonlocal damped nano-beams on elastic foundation. Eur J Mech / A Solids 86:104144
48. Mamaghani AE, Sarparast H, Rezaei M (2020) On the vibrations of axially graded Rayleigh beams under a moving load. Appl Math Modell 84:554–570
49. Kou KP, Yang Y (2019) A meshfree boundary-domain integral equation method for free vibration analysis of the functionally graded beams with open edged cracks. Composites Part B 156:303–309
50. Cui DF, Hu HY (2014) Thermal buckling and natural vibration of the beam with an axial stick-slip-stop boundary. J Sound Vib 333:2271–2282
51. Bourhis EL (2014) Glass mechanics and technology. Wiley-VCH Verlag GmbH & Co. KGaA, Boschstr. 12 69469 Weinheim, Germany
52. Caddemi S, Calio I (2009) Exact closed-form solution for the vibration modes of the Euler-Bernoulli beam with multiple open cracks. J Sound Vib 327:473–489